Soft-x-ray spectroscopy of $\Delta n = 0$, $n = 3$ transitions in highly stripped lead

A. Simionovici,* D. D. Dietrich, R. Keville, T. Cowan, P. Beiersdorfer, M. H. Chen, and S. A. Blundell†
Lawrence Livermore National Laboratory, Livermore, California 94550
(Received 10 May 1993)

We report on $n = 3$ to $n = 3$ soft-x-ray transitions from the highest nuclear charge ($Z = 82$) Na-like ions yet obtained. The results are tied to accurate calculations including screened QED contributions and confirm theoretical trends observed by Kim *et al.* [Phys. Rev. A **44**, 148 (1991)]. Weak Ne-like and Mg-like lines are observed in an accelerator-based experiment in the energy range near 800 eV and compared to multiconfiguration Dirac-Fock calculations.

PACS number(s): 32.30.Rj, 12.20.Fv, 31.20.Di, 31.30.Jv

I. INTRODUCTION

The evolution of precision spectroscopy of few-electron high-Z ions in recent years has followed the availability of these ions from facilities the world over. With the production of H- and He-like beams of elements from xenon to uranium at the Bevalac, GANIL and GSI, attention is shifting to studies of increasingly complex systems. Recently, there has been considerable interest in the spectroscopy of Ne- and Na-like ions of the highest available atomic number. Theoretical calculations [1–4], semiempirical corrections [5,6] and experiments [7–14] reported results on ions between $Z = 42$ (Mo) and $Z = 83$ (Bi).

In the following we report the first observation of the sodiumlike $3p_{3/2} \rightarrow 3s_{1/2}$ and $3d_{3/2} \rightarrow 3p_{1/2}$ transitions in a very highly charged ion, Pb^{71+} from an accelerator source, the Unilac accelerator at the GSI facility in Darmstadt. Among these transitions, the Na-like $3p_{3/2} \rightarrow 3s_{1/2}$ transition is of special interest because it is strongly affected by quantum electrodynamical (QED) effects. Theoretical efforts based on the multiconfiguration Dirac-Fock (MCDF) [4] or the relativistic many-body perturbation theory (RMBPT) [1] methods have obtained relativistic transition energies including high-order electron-correlation effects and the Breit interaction with precision better than 0.1 eV. The remaining problem to be solved involves accurate predictions of the QED corrections. Recently, Cheng, Johnson, and Sapirstein [15] and Blundell [16] worked out "screened" QED corrections in an *ab initio* manner for the single-valence electron Na-like system, while comparable results were obtained from predictions estimated by smoothing out the differences between theoretical calculations and selected experiments [4]. Measurements of the $3p_{3/2} \rightarrow 3s_{1/2}$ transition energy thus provide tests of the accuracy of the different approaches developed to predict the QED contribution.

The $\Delta n = 0$, $n = 3$ transitions fall into the soft-x-ray region near 800 eV. This required the construction of a spectrometer that not only is sensitive to such low-energy photons, but one that minimizes the production of and sensitivity to low-energy background fluorescence x rays. This background fluorescence radiation is produced by the hard x rays emitted by the Unilac's multi-MeV ions and by the Bremstrahlung from those δ electrons which stop in the target chamber. As the intensity of the fluorescence x rays is easily capable of overwhelming the line radiation of interest, a major effort was required to minimize this source of background. The present experiment achieved a signal-to-noise ratio of 1:3. This was sufficient to identify the sodiumlike lines and to perform an accurate determination of their energy separation. With the help of theoretical oscillator strengths we have constructed synthetic spectra that were used to tentatively identify several $n = 3 \rightarrow n = 3$ (3-3) transitions from ions in the neighboring neonlike and magnesiumlike charge states. Measurements of transitions in these ions challenge theory to provide accurate predictions for open-shell ions and thus complement measurements of transitions in the sodiumlike ion, which has only a single valence electron outside a closed shell.

II. EXPERIMENT

Our experimental apparatus was mounted on the $X2$ beam line of the Unilac accelerator in GSI, Darmstadt in a setup described elsewhere [8]. Fourteen MeV/amu Pb ions were produced by the Unilac and passed through a thick (~ 600 $\mu g/cm^2$) C stripper foil. Lead beams of charge states 66+, 72+, and 73+ were then charge analyzed through a magnetic spectrometer and impinged onto 200-$\mu g/cm^2$ C targets. Figure 1 shows the measured charge-state distribution delivered by the Unilac, compared with semiempirical predictions based on a modified expression of the Nikolaev and Dimitriev formula [17]. Beam profilers mounted in the beam line before and after our spectrometer are checked before, after, and during a run to ensure stability of the beam alignment. A Faraday cup, mounted at the end of the beam line serves as an absolute reference of the beam current which was about 15 electrical nA for all the incident charge states. Three incident charge states used allowed us to vary the experimental conditions of production of the wanted species and thus to reduce systematic errors. Electron capture to excited states, innershell ionization, and excitation were the main population mechanisms in order of decreasing importance.

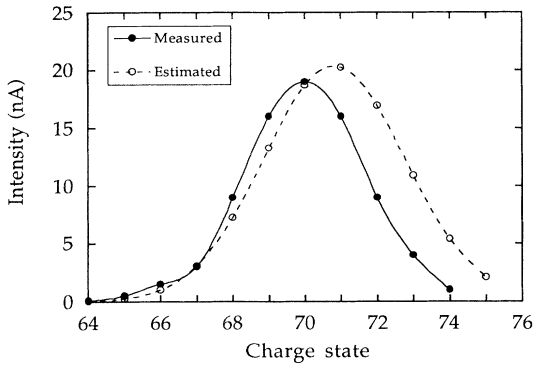

FIG. 1. Measured and estimated (normalized) charge-state distributions for 14-MeV/amu Pb after a 600-μg/cm^2 C foil.

The experimental apparatus used was the LLNL dual Johann spectrometer modified to accept two movable active (MCP) detectors. The instrument was redesigned to use a 60-cm-radius curved rubidium acid phthalate crystal (RbAP) in three different Bragg geometries of incidence angles of 35° to 45°. A schematic of the instrument is shown in Fig. 2. Throughout the duration of an exposure, the position of the exciter foil is imaged through a set of two slits located in the instrument plane on two proportional counters placed on both sides of the spectrometer. By maximizing the counting rate on the proportional counters, the foil position along the beam direction is tracked with an accuracy on the order of 100–200 μm. A previously aligned thin tungsten wire of high absorption coefficient, centered in front of the MCP's, casts a shadow onto the face of the detector. This serves to locate the position of the instrument plane (zero linear Doppler shift) on the MCP's. A miniature x-ray tube can be remotely inserted in front of the crystals, in the position of the exciter foil. Electron-beam bombardment of powdered elements (Fe,Co) attached to the anode using silver epoxy, provides a convenient source of calibration x rays. The Fe and Co $K\alpha$ and $K\beta$ lines in eighth and ninth refraction orders and $L\alpha$ and $L\beta$ in first order were used in the calibration. Short exposures (5–10 min) with this source are performed periodically to track the stability of the overall system calibration. The x-ray source is removed and the foil is moved into position. The linear Doppler shift can in principle be eliminated by averaging out the spectra obtained on the two symmetric MCP's and only the second-order corrections due to the beam velocity (γ) are applied. In our experiment, due to technical problems, only one MCP was used, consequently the spectra obtained had to be corrected for both the first- and second-order Doppler shifts.

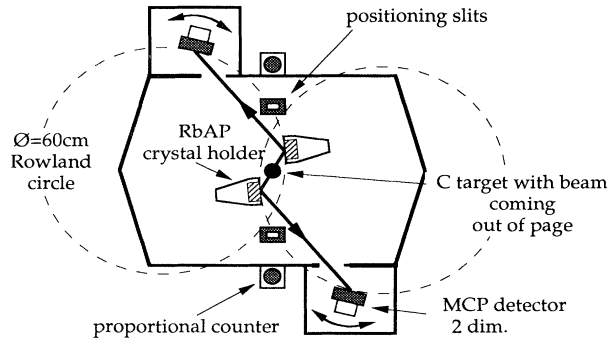

FIG. 2. Schematic of the double Johann instrument.

By far the largest experimental obstacle was due to the tremendous soft-x-ray background in the spectrometer. Both hard (multi-keV) and soft x rays are produced in the interaction of the lead beam with the C target and also from the bremstrahlung and characteristic line radiation produced when δ electrons are stopped in the target chamber. This radiation in turn produces lower-energy fluorescence x rays. While the detector could be shielded from unwanted primary x rays, it was impossible to shield it from the secondary fluorescent photons such as those given off by the crystal holder. As a result, it was necessary to cover every surface within the spectrometer, except the crystal, with foils of successively lower-Z material (e.g., Cu-Al-C). High-energy x rays penetrate the low-Z foil on the outside and interact with the high-Z material on the inside generating K- and L-shell x rays of successively lower energy in the backward direction, which are then largely absorbed by the outer carbon layer. Use of this graded-Z shielding technique reduced the soft-x-ray background, as seen by the detector, by orders of magnitude.

III. LINE IDENTIFICATION

A typical spectrum is shown in Fig. 3(a). The spectrum was obtained in a single run after approximately 80 min of exposure with the 73+ incident charge state. The high background is caused by residual low-energy x rays scattered into the detector. Three such spectra produced by 72+ or 73+ incident charge states were recorded. For comparison, a spectrum produced by the 66+ incident charge state is shown in Fig. 3(b). We expect features due to sodiumlike lead or those from neighboring charge states to be absent for such a low incident charge state, which is indeed the case. Moreover, the spectrum allows us to assess the uniformity of the detector response to the scattered background radiation.

In the spectra produced by the 72+ or 73+ incident charge states we identify the two features marked 3 and 6 as the sodiumlike $3p_{3/2}\rightarrow 3s_{1/2}$ and $3d_{3/2}\rightarrow 3p_{1/2}$ transitions, respectively. The identification is based on their positions as well as their relative intensities. Using the calibration lines from the built-in miniature x-ray tube we can determine their energies to within about 0.5 eV, and a good match with theoretical predictions is found. An overview of the measured energies of the two lines from the three different spectra we observed is given in Table I. The ratio of the predicted oscillator strengths of the $3p_{3/2}\rightarrow 3s_{1/2}$ and $3d_{3/2}\rightarrow 3p_{1/2}$ transitions is 1.4:1; the ratio of the observed intensities of features 3 and 6 is 2:1. The difference may simply be due to the fact that oscillator strengths are poor indicators of the population mechanisms of the upper levels; overlap with transitions in

neighboring charge states may also cause part of the difference, as discussed below.

In order to identify the remaining features marked 1, 2, 4, and 5 in the spectrum in Fig. 3(a) we have constructed a synthetic spectrum of the five dominant lines from each, F-like, Mg-like, and Al-like lead charge states using normalized oscillator strengths as intensities, and linewidths similar to those measured in the experimental spectra. (Lines from the Ne-like charge state are discussed separately below.) The transition energies for F-like, Mg-like, and Al-like were calculated using the MCDF code of Grant *et al.* [18] in the average level (AL) mode. In this mode the orbital energies are obtained minimizing the averaged energy of all the levels with equal weights. These calculations were carried out in intermediate coupling with configuration interaction from the same complex. The nucleus is assumed to have a uniform charge distribution. In our present work we used 110, 35, and 148 configurations for the F-like, Mg-like and Al-like lead, respectively. The resulting synthetic spectrum is shown in Fig. 4. Vertical bars mark the positions of features 1–6 from Fig. 3(a). Contributions from Al-like ions (solid lines) are ruled out by the absence of an observed feature around 785 or 808 eV. By contrast, contributions from Mg-like ions (short-dashed line) appear likely, though small, and are indicated by the observed feature labeled 1. Contributions from F-like transitions (long-dashed line) cannot be ruled out and may add to features 1–4 in our spectra. However, population of $n=3$ F-like levels from an incident F-like beam (73+) is a rather unlikely mechanism. It would occur either as a two-step process, i.e., capture into $n=3$ followed by innershell ionization, or through direct excitation. By contrast, the dominant processes are captured into $n=2$

TABLE I. Energies of features 3 and 6 for three different spectra. The features are predominantly ascribed to the Na-like $3p_{3/2}\rightarrow 3s_{1/2}$ and $3d_{3/2}\rightarrow 3p_{1/2}$ transition, respectively. The energies were determined relative to calibration lines from an internal x-ray tube.

Spectrum	Energy (eV)	Systematic errors (eV)	Statistical errors (eV)
	Line 3		
1	798.68	0.43	0.15
2	798.29	0.44	0.15
3	798.91	0.44	0.17
	Line 6		
1	823.23	0.34	0.18
2	822.77	0.36	0.22
3	823.24	0.36	0.22

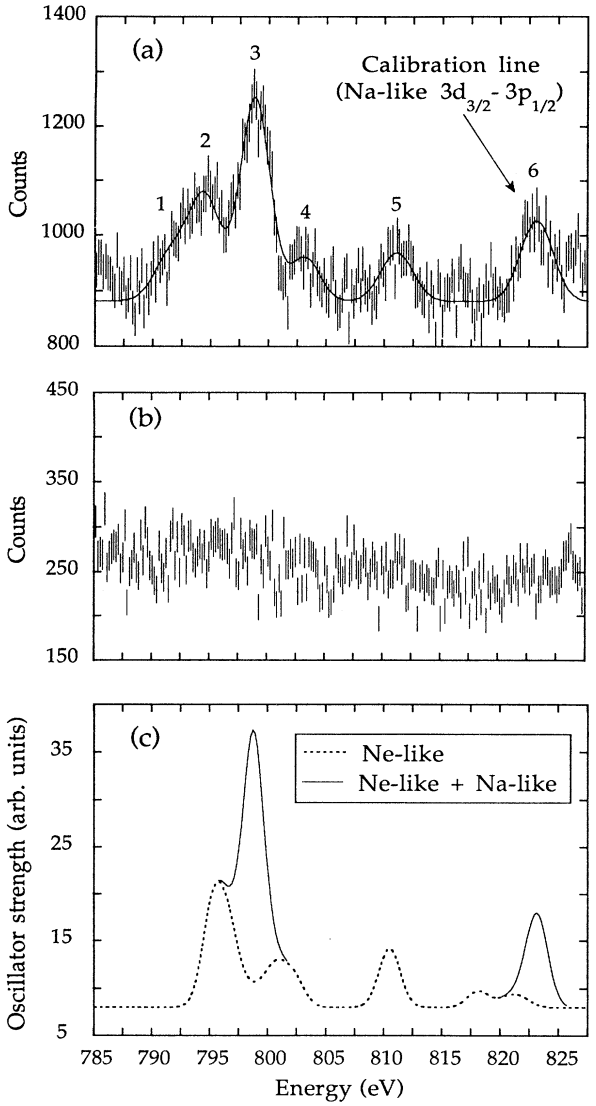

FIG. 3. Spectra obtained with (a) Pb^{73+} incident beam (80 min exposure) and (b) Pb^{66+} incident beam (45 min exposure). The six features labeled in (a) are fitted by Gaussian profiles and discussed in the text. (c) A synthetic spectrum based on the oscillator strengths of Na-like and Ne-like lines, as discussed in the text. The contribution from the Ne-like charge state is the dashed line.

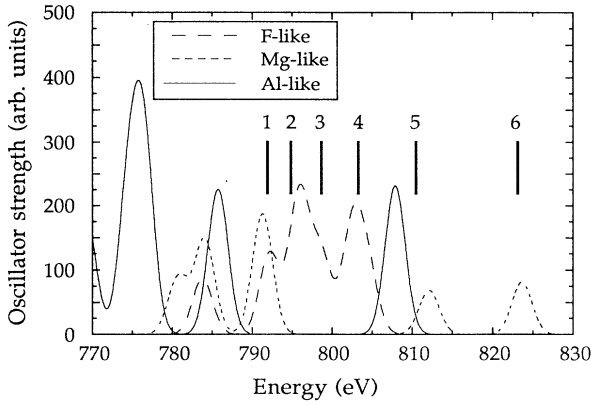

FIG. 4. Synthetic spectrum based on oscillator strengths showing transitions from F-like (long-dashed line), Mg-like (short-dashed line), and Al-like (solid line) lead. The positions of the measured features are indicated with vertical bars and labeled as in Fig. 3.

levels and ionization of the outer-shell electrons. Thus, F-like ions are most likely produced in the ground state. In our subsequent discussion we presume that the F-like transition contributes negligibly to the observation. Instead, we attribute the features 2, 4, and 5 to transitions in Ne-like ions as discussed in the following.

In Fig. 3(c) we show a synthetic spectrum constructed from the Ne-like and Na-like transitions and compare it to the Gaussian fit of features 1–6. Again, calculations of the energy levels and oscillator strengths were performed with the code of Grant *et al.* [18] in the AL mode. In order to generate the synthetic spectrum shown in Fig. 3(c) we decreased the line strengths of the Ne-like and Na-like $3d_{3/2}\rightarrow 3p_{1/2}$ lines by 3 and 1.5, respectively, relative to the strength of the corresponding $3p_{3/2}\rightarrow 3s_{1/2}$ transitions. Doing so provides a synthetic spectrum that matches the observed features well [cf. Figs. 3(a) and 3(c)]. A listing of the Ne-like transitions included in the construction of the synthetic spectrum is given in Table II. All quantities (transition energy, radiative branching ratio, and absorption oscillator strength) were calculated with the MCDF code of Grant *et al.* [18]. Only Ne-like 3-3 transitions that involve a $2p$ vacancy were included in constructing the synthetic spectrum. Those involving a $2s$ vacancy were not included. Three of these could contribute, namely, the transitions

$$(2s_{1/2}^{-1}3p_{3/2})_{J=2}\rightarrow(2s_{1/2}^{-1}3s_{1/2})_{J=1}\ ,$$

$$(2s_{1/2}^{-1}3d_{3/2})_{J=2}\rightarrow(2s_{1/2}^{-1}3p_{1/2})_{J=0}\ ,$$

and

$$(2s_{1/2}^{-1}3d_{3/2})_{J=1}\rightarrow(2s_{1/2}^{-1}3p_{1/2})_{J=1}\ ,$$

with energies 803.5, 810.0, and 811.1 eV and oscillator strengths 0.18, 0.24, and 0.13, respectively. However, they must compete with $2p\rightarrow 2s$ transitions, and are unlikely to take place.

Comparing the synthetic spectrum in Fig. 3(c) with the data in Fig. 3(a) we identify features 2, 4, and 5 as Ne-like lines, and predict contributions from Ne-like transitions to the two Na-like features 3 and 6.

IV. QED CONTRIBUTION AND COMPARISON WITH THEORY

The external energy calibration of our spectra with the miniature x-ray tube provides an accuracy of about 0.5 eV. The accuracy is limited by systematic errors resulting from the bidimensional image processing, beam misalignment, and the beam energy. By relying on an internal wavelength reference, we can eliminate the contributions from systematic errors that are common to all spectral features.

The Na-like $3d_{3/2}\rightarrow 3p_{1/2}$ line represents an ideal internal reference line, as it features the lowest QED contribution and its non-QED energy is well understood and accurately calculated in the framework of the relativistic many-body perturbation method (RMBPT) [1]. In particular, we used the RMBPT code of Johnson, Blundell, and Sapirstein [1] to calculate its energy of 823.17 eV, which includes an *ab initio* QED correction of -0.81 eV determined with the method described in Ref. [16]. The value of any uncalculated contributions is estimated to be less than 0.05 eV, and we assign a 0.1 eV confidence limit to the line's theoretical energy. Assigning this energy to feature 6, we determine the energy of the other five features in our spectra. The results are listed in Table III. The uncertainty of each energy value is determined by the quadratic sum of the statistical uncertainty in the line position (including that of the reference peak). Any error in the theoretical value of the reference line is not included. A possible drawback of this calibration procedure is given by the possibility that feature 6 is not solely due to the Na-like $3d_{3/2}\rightarrow 3p_{1/2}$ transition but also contains contributions from the two Ne-like $3d\rightarrow 3p$ transitions that we predicted to have energies (820.6 and 821.8 eV, respectively) close to that of the Na-like line. This possibility increases the overall uncertainty by an unknown amount; however, since the intensity of the Ne-like $3d\rightarrow 3p$ lines appear to be weak, we expect the

TABLE II. Transitions in Ne-like Pb^{72+} contributing to the synthetic spectrum in Fig. 3(c). The radiative branching ratio is denoted β_r, the transition energy by E, and the absorption oscillator strength by gf.

Transition	β_r	E (eV)	gf
$(2p_{3/2}^{-1}3p_{3/2})J=3\rightarrow(2p_{3/2}^{-1}3s_{1/2})J=2$	1.00	795.3	1.13
$(2p_{3/2}^{-1}3p_{3/2})J=1\rightarrow(2p_{3/2}^{-1}3s_{1/2})J=2$	0.15	796.1	0.07
$(2p_{1/2}^{-1}3p_{3/2})J=2\rightarrow(2p_{1/2}^{-1}3s_{1/2})J=1$	0.70	796.7	0.81
$(2p_{1/2}^{-1}3p_{3/2})J=1\rightarrow(2p_{1/2}^{-1}3s_{1/2})J=1$	0.33	798.8	0.18
$(2p_{3/2}^{-1}3p_{3/2})J=2\rightarrow(2p_{3/2}^{-1}3s_{1/2})J=1$	0.36	800.6	0.41
$(2p_{3/2}^{-1}3d_{3/2})J=0\rightarrow(2p_{3/2}^{-1}3p_{1/2})J=1$	1.00	801.0	0.14
$(2p_{1/2}^{-1}3p_{3/2})J=1\rightarrow(2p_{1/2}^{-1}3s_{1/2})J=0$	0.67	802.3	0.34
$(2p_{3/2}^{-1}3p_{3/2})J=2\rightarrow(2p_{3/2}^{-1}3s_{1/2})J=2$	0.37	810.5	0.42
$(2p_{3/2}^{-1}3d_{3/2})J=3\rightarrow(2p_{3/2}^{-1}3p_{1/2})J=2$	1.00	810.5	0.81
$(2p_{1/2}^{-1}3d_{3/2})J=2\rightarrow(2p_{1/2}^{-1}3p_{1/2})J=1$	1.00	818.2	0.58
$(2p_{3/2}^{-1}3d_{3/2})J=2\rightarrow(2p_{3/2}^{-1}3p_{1/2})J=2$	0.50	820.6	0.30
$(2p_{3/2}^{-1}3d_{3/2})J=2\rightarrow(2p_{3/2}^{-1}3p_{1/2})J=1$	0.50	821.8	0.29

TABLE III. Comparison of measured and calculated transition energies. The experimental energies are determined relative to the Na-like $3d_{3/2} \rightarrow 3p_{1/2}$ transition at 823.12 eV. The theoretical energies are calculated with the code of Grant *et al.*, Ref. [18]. An asterisk denotes dominant transition in each feature. The errors shown are statistical and do not account for blends.

Feature	Charge state	Transition	Experiment (eV)	Theory (eV)
1	*Mg-like	$(3d_{3/2}\,3p_{3/2})_{J=3} \rightarrow (3d_{3/2}\,3s_{1/2})_{J=2}$	791.90±0.29	791.3
2	Ne-like	$(2p_{3/2}^{-1}\,3p_{3/2})_{J=3} \rightarrow (2p_{3/2}^{-1}\,3s_{1/2})_{J=2}$	794.85±0.22	795.3
	Ne-like	$(2p_{3/2}^{-1}\,3p_{3/2})_{J=1} \rightarrow (2p_{3/2}^{-1}\,3s_{1/2})_{J=2}$		796.1
	Ne-like	$(2p_{1/2}^{-1}\,3p_{3/2})_{J=2} \rightarrow (2p_{1/2}^{-1}\,3s_{1/2})_{J=1}$		796.7
3	*Na-like	$3p_{3/2} \rightarrow 3s_{1/2}$	798.65±0.13	799.5
	Ne-like	$(2p_{1/2}^{-1}\,3p_{3/2})_{J=1} \rightarrow (2p_{1/2}^{-1}\,3s_{1/2})_{J=1}$		798.8
	Ne-like	$(2p_{3/2}^{-1}\,3p_{3/2})_{J=2} \rightarrow (2p_{3/2}^{-1}\,3s_{1/2})_{J=1}$		800.6
	Ne-like	$(2p_{3/2}^{-1}\,3d_{3/2})_{J=0} \rightarrow (2p_{3/2}^{-1}\,3p_{1/2})_{J=1}$		801.0
4	*Ne-like	$(2p_{1/2}^{-1}\,3p_{3/2})_{J=1} \rightarrow (2p_{1/2}^{-1}\,3s_{1/2})_{J=0}$	803.27±0.51	802.3
5	*Ne-like	$(2p_{3/2}^{-1}\,3p_{3/2})_{J=2} \rightarrow (2p_{3/2}^{-1}\,3s_{1/2})_{J=2}$	810.48±0.19	810.5
	Ne-like	$(2p_{3/2}^{-1}\,3d_{3/2})_{J=3} \rightarrow (2p_{3/2}^{-1}\,3p_{1/2})_{J=2}$		810.5

amount to be small, and this uncertainty is not added to the overall uncertainty. Furthermore, we note that we cannot rule out small energy shifts for each transition deriving from $n=4,5\ldots$ spectator electrons. Our data are of insufficient quality to warrant detailed investigation of such possibilities.

A comparison with energies calculated with the code of Grant *et al.* [18] shows agreement better than about 1 eV. This is in accord with the predictive accuracy of MCDF calculations determined in comparison with measurements of Ne-like, Na-like, Mg-like, and Al-like $3 \rightarrow 2$ transitions [19].

From our data we can extract an energy for the Na-like $3p_{3/2} \rightarrow 3s_{1/2}$ transition. This line overlaps with Ne-like transitions to produce feature 3. Using the results of our model spectrum [Fig. 3(c)] we subtract the estimated contribution from the Ne-like lines. This shifts the centroid of feature 3 by 0.11 eV. The shift, of course, may be larger or smaller depending on the actual intensity and position of the Ne-like lines. Similarly, if F-like lines overlapped the Na-like line (cf. Sec. III), the centroid of feature 3 may also be shifted, though in the opposite direction. In the following we apply half of the 0.11 eV shift to the energy measured for feature 3 and increase the uncertainty in quadrature by 0.11 eV. The value of the Na-like $3p_{3/2} \rightarrow 3s_{1/2}$ transition we thus infer from our data relative to the theoretical energy of the $3d_{3/2} \rightarrow 3p_{1/2}$ transition is 798.65±0.18 eV. We can compare our value to several values calculated with different theoretical techniques. We calculated the energy of the Na-like $3p_{3/2} \rightarrow 3s_{1/2}$ transition with the RMBPT code of Johnson, Blundell, and Sapirstein [1] and found a value of 798.76 eV. This value includes −6.46 eV due to QED corrections calculated *ab initio* with the method described by Blundell [16]. The RMBPT energy agrees well with our measurement. It is also in excellent agreement with the 798.81-eV transition energy predicted by Kim *et al.* [4]. A semiempirical calculation by Seely *et al.*, [6], which makes use of Grant's QED contributions [20] added to the RMBPT values [1], predicts −5.97 eV for the QED value. Seely *et al.* [6] find a value of 799.13 eV for the Na-like $3p_{3/2} \rightarrow 3s_{1/2}$ transition, which is significantly larger than measured. For completeness, we note that Kim and Mohr's [21,22] hydrogenic QED value is −8.73 eV, which is larger (as expected) than the screened QED contributions discussed above.

V. CONCLUSION

We obtained spectra of 3-3 transitions in highly charged lead using the beam-foil method. The two dominant features are assigned to Na-like transitions, while several weak features are assigned to Mg-like and Ne-like transitions. The transitions fall into the ultrasoft-x-ray region near 800 eV. This presents special experimental difficulties which were discussed in detail. In particular, a high background reduced the signal-to-noise ratio and precluded definitive checks of the assumptions that entered into the model used for line identification. Based on our experience, experiments may be devised that provide precision data of a variety of transitions in highly charged ions that fall into this energy region. Among these, the Ne-like $3 \rightarrow 3$ transitions are most noteworthy. These have not been observed in plasma observations or from x-ray sources such as the electron beam ion trap [13], as the cross sections for electron-impact excitation of $n=3$ levels are much smaller for Ne-like ions than, for example, for Na-like ions. The beam-foil method thus has an advantage, because $n=3$ may be predominantly

populated by electron capture instead of electron-impact excitation.

ACKNOWLEDGMENTS

This work was performed under the auspices of the Department of Energy by the Lawrence Livermore National Laboratory under Contract No. W-7405-ENG-48. A.S. and D.D.D. acknowledge support under NATO Grant No. CRG900630. A.S. is grateful to W. R. Johnson for the loan of the RMBPT codes and for helpful discussions. The authors would like to thank the GSI staff who provided optimal conditions for the experiment.

*Present address: LAGRIPPA, CENG, BP 85X, Grenoble, France.

†Present address: LI2A, CENG, BP 85X, Grenoble, France.

[1] W. R. Johnson, S. A. Blundell, and J. Sapirstein, Phys. Rev. A **38**, 2699 (1988).

[2] D. H. Baik, Y. G. Ohr, K. S. Kim, J. M. Lee, P. Indelicato, and Y.-K. Kim, At. Data Nucl. Data Tables **47**, 177 (1991).

[3] M. H. Chen, Nucl. Instrum. Methods Phys. Res., Sect. B **43**, 366 (1989).

[4] Y.-K. Kim, D. H. Baik, P. Indelicato, and J. P. Desclaux, Phys. Rev. A **44**, 148 (1991).

[5] J. F. Seely and R. A. Wagner, Phys. Rev. A **41**, 5246 (1990).

[6] J. F. Seely, C. M. Brown, U. Feldman, J. O. Ekberg, C. J. Keane, B. J. MacGowan, D. R. Kania, and W. E. Behring, At. Data Nucl. Data Tables **47**, 1 (1991).

[7] J. Reader, V. Kaufman, J. Sugar, J. O. Ekberg, U. Feldman, C. M. Brown, J. F. Seely, and W. L. Rowan, J. Opt. Soc. Am. B **4**, 1821 (1987).

[8] D. D. Dietrich, A. Simionovici, M. H. Chen, G. Chandler, C. J. Hailey, P. O. Egan, P. H. Mokler, S. Reusch, and D. H. H. Hoffmann, Phys. Rev. A **41**, 1450 (1990).

[9] J. F. Seely, U. Feldman, C. M. Brown, M. C. Richardson, D. D. Dietrich, and W. E. Behring, J. Opt. Soc. Am. B **5**, 785 (1988).

[10] D. D. Dietrich, G. A. Chandler, P. O. Egan, K. P. Ziock, P. H. Mokler, S. Reusch, and D. H. H. Hoffmann, Nucl. Instrum. Methods Phys. Res., Sect. B **24/25**, 301 (1987).

[11] G. A. Chandler, M. H. Chen, D. D. Dietrich, P. O. Egan, K. P. Ziock, P. H. Mokler, S. Reusch, and D. H. H. Hoffmann, Phys. Rev. A **39**, 565 (1989).

[12] P. Beiersdorfer, S. von Goeler, M. Bitter, E. Hinnov, R. Bell, S. Bernabei, J. Felt, K. W. Hill, R. Hulse, J. Stevens, S. Suckewer, J. Timberlake, A. Wouters, M. H. Chen, J. H. Scofield, D. D. Dietrich, M. Gerassimenko, E. Silver, R. S. Walling, and P. L. Hagelstein, Phys. Rev. A **37**, 4153 (1988).

[13] T. E. Cowan, C. L. Bennet, D. D. Dietrich, J. V. Bixler, C. J. Hailey, J. R. Henderson, D. A. Knapp, M. A. Levine, R. E. Marrs, and M. B. Schneider, Phys. Rev. Lett. **66**, 1150 (1991).

[14] P. Beiersdorfer, M. H. Chen, R. E. Marrs, and M. A. Levine, Phys. Rev. A **41**, 3453 (1990).

[15] K. T. Cheng, W. R. Johnson, and J. Sapirstein, Phys. Rev. Lett. **23**, 2960 (1991).

[16] S. A. Blundell, Phys. Rev. A **46**, 3762 (1992); **47**, 1790 (1993).

[17] V. S. Nikolaev and I. S. Dmitriev, Phys. Lett. **28A**, 277 (1968).

[18] I. P. Grant, B. J. McKenzie, P. H. Norrington, D. F. Mayers, and N. C. Pyper, Comput. Phys. Commun. **21**, 207 (1980).

[19] P. Beiersdorfer, M. Bitter, S. von Goeler, S. Cohen, K. W. Hill, J. Timberlake, R. S. Walling, M. H. Chen, P. L. Hagelstein, and J. H. Scofield, Phys. Rev. A **34**, 1297 (1986).

[20] B. J. McKenzie, I. P. Grant, and P. H. Norrington, Comput. Phys. Commun. **21**, 233 (1980).

[21] P. J. Mohr and Y. K. Kim, Phys. Rev. A **45**, 2727 (1992).

[22] Mohr's and Kim's self-energy was fitted to obtain the value $E_{SE}(Z=82)=-10.397$ eV. The vacuum polarization correction of $E=1.67$ eV was added to obtain the total QED value $E_{QED}=-8.727$ eV.